npj computational materials

www.nature.com/npjcompumats

ARTICLE OPEN

Check for updates

Superconductivity in unconventional metals

Zhilong Yang[1,2,3], Haohao Sheng[1,2,3], Zhaopeng Guo[1,2], Ruihan Zhang[1,2], Quansheng Wu[1,2], Hongming Weng[1,2], Zhong Fang[1,2] and Zhijun Wang[1,2]✉

Based on first-principles calculations, we demonstrate that 1H/2H-phase transition metal dichalcogenides MX_2 (M = Nb, Ta; X = S, Se, Te) are unconventional metals, which have an empty-site band of A_1'@1e elementary band representation at the Fermi level. The computed phonon dispersions indicate the stability of the system at high temperatures, while the presence of the soft phonon mode suggests a phase transition to the charge density wave state at low temperatures. Based on the Bardeen-Cooper-Schrieffer theory and computed electron-phonon coupling, our calculations show that the superconductivity (SC) in $NbSe_2$ is mainly attributed to the soft phonon mode due to the half filling of the empty-site band. Accordingly, the SC has been predicted in unconventional metals TaNS monolayer and 2H-TaN_2 bulk with computed T_C = 10 K and 26 K respectively. These results demonstrate that the unconventional metals with partial filling of the empty-site band offer an attractive platform to search for superconductors.

npj Computational Materials (2024)10:25 ; https://doi.org/10.1038/s41524-024-01210-z

INTRODUCTION

In the past decades, topological materials have attracted a lot of attention due to their novel properties in condensed matter physics[1–12]. Most recently, a new kind of unconventional materials has been proposed to be topologically trivial with wannierizable valence Bloch states, while they have a set of bands from an elementary band representation (EBR) on an empty site[13–15]. The unconventional insulators are also known as obstructed atomic insulators[16–19]. Besides, there are also many unconventional metals, such as electrides[14], catalysis[20], solid-state hydrogen storage[13], and superconductivity, etc[21,22].

Transition metal dichalcogenides (TMD), such as hexagonal bilayer stackings of dichalcogenides, named 2H-MX_2, have received attention with the discovery of charge density wave (CDW) and superconductivity (SC). The CDW transition temperature decreases from around 120 K in 2H-$TaSe_2$, to 80 K in 2H-TaS_2, down to 30 K in 2H-$NbSe_2$ and finally no CDW in 2H-NbS_2[23,24]. The superconducting critical temperature T_C increases from around 0.2 K in 2H-$TaSe_2$ up to 7.2 K and 6 K in 2H-$NbSe_2$ and 2H-NbS_2, respectively. Although these properties have been widely studied in literature, the origin of the SC has not been revealed yet.

In this work, based on first-principles calculations and band representation analysis, we demonstrate that the monolayer 1H-MX_2 is an unconventional metal, with a half-filling EBR at an empty 1e site. The real space invariant (RSI) of the empty site is δ_1@1e = 1. The computed phonon dispersions show CDW instability at low temperatures. Based on the Bardeen-Cooper-Schrieffer (BCS) theory, the computed electron-phonon coupling (EPC) suggests the SC is attributed to soft phonon mode. The results reveal that the partial filling of the empty-site band gives rise to the strong EPC and potential SC. Following the strategy, two superconductors, TaNS monolayer and 2H-TaN_2 bulk, have been predicted with T_C = 10 K and 26 K respectively.

RESULTS AND DISCUSSION

Unconventional electronic band structure

The 2H-MX_2 possesses a hexagonal structure with a space group (SG) of $P6_3/mmc$, where a hexagonal plane of M atoms is sandwiched by two layers of X atoms in Fig. 1a. The MX_2 monolayers are connected by van der Waals force. For convenience, we mainly focus on the monolayer 2H-MX_2 (1H-phase). The M and X are located at the 1c and 2g Wyckoff positions of SG 187. Based on the atomic configurations, the atomic valence-electron band representations (ABRs) are generated by POS2ABR in Table 1.

The computed band structures of $NbSe_2$ and TaS_2 are presented in Fig. 1b, c, respectively. The computed irreducible representations of energy bands indicate that the six lower energy bands belong to ABR $(A_1 + E)$@2g, corresponding to the p states of chalcogens in Table 1. An isolated band at E_F belongs to A_1'@1e EBR with a half filling. The RSI of the empty 1e Wyckoff site is δ_1@1$e \equiv m(A_1') + m(A_1'') - m(A_2') - m(A_2'') - m(E') + m(E'') = 1$, with $m(\rho)$ is the number of EBR ρ@1e. Due to the presence of C_3 symmetry[25], the Jenus 1H-TaSeS is also defined as an unconventional metal, and its superconductivity has been confirmed in experiment[26].

Formation of the empty-site EBR at E_F

In a compound, all electronic states should originate from the ABRs[13]. The orbital-resolved band structures of representative $NbSe_2$ in Fig. 2b show the Fermi-level band is consist of Nb-d_{z^2} and Nb-d_{xy,x^2-y^2}, which induce A_1'@1c and E'@1c ABRs, respectively. The band representations of topological quantum chemistry theory show

$$A_1'@1c + E'@1c = A_1'@1e + E'@1e. \quad (1)$$

Therefore, we conclude that the hybridization of the two ABRs gives rise to half occupied EBR A_1'@1e and unoccupied EBR E'@1e, as illustrated in Fig. 2a. In 1H-(Nb,Ta)X_2, the empty-site EBR A_1'@1e is half filled, resulting in an unconventional metal. In the Na_xNbX_2

[1]Beijing National Laboratory for Condensed Matter Physics, and Institute of Physics, Chinese Academy of Sciences, 100190 Beijing, China. [2]University of Chinese Academy of Sciences, 100049 Beijing, China. [3]These authors contributed equally: Zhilong Yang, Haohao Sheng. ✉email: wzj@iphy.ac.cn

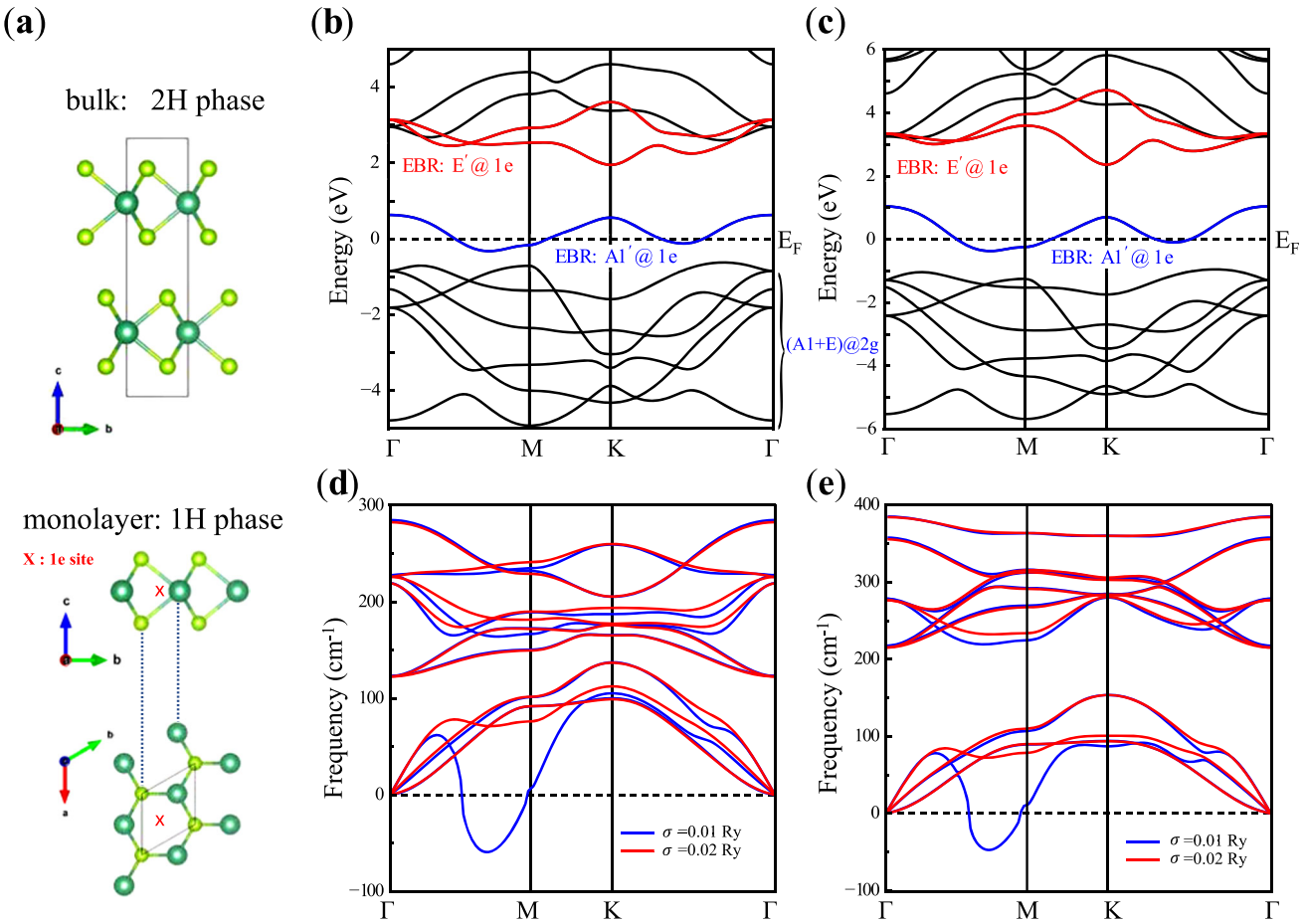

Fig. 1 The crystal structures, electronic structures, and phonon dispersions of 1H-MX_2. **a** Crystal structure of 1H-MX_2. **b**, **c** Electronic structures of $NbSe_2$ and TaS_2. **d**, **e** Phonon dispersions of $NbSe_2$ and TaS_2 with different electronic smearing parameters (σ).

Table 1. The atomic valence-electron band representations (ABRs) of 1H-MX_2.

Atom	WKS(q)	Symm.	Conf.	Irreps(ρ)		ABRs (ρ@q)	Occ.
Nb	1c	-62m	d^5	d_{z^2}:	A_1'	A_1'@1c	
(M)	$(\frac{1}{3}\frac{2}{3}0)$			d_{xy,x^2-y^2}:	E'	E'@1c	
				$d_{xz,yz}$:	E''	E''@1c	
Se	2g	3m	p^4	p_z:	A_1	A_1@2g	yes
(X)	(00z)			p_x, p_y:	E	E@2g	yes
	1e			A_1'@1e : empty-site EBR			
	$(\frac{2}{3}\frac{1}{3}0)$						half-filled

The ABRs are defined as the band representations induced by the atomic valence electrons. The Nb d orbitals form the A_1', E', and E'' irreps at the Nb(1c) site, being A_1'@1c, E'@1c, and E''@1c ABRs, while the Se p orbitals form the A_1, and E irreps at the Se(2g) site, being A_1@2g and E@2g ABRs.

and $Mo_xNb_{1-x}X_2$, this empty-site EBR becomes fully occupied at $x = 1$, resulting in an unconventional insulator/obstructed atomic insulator[13,14,16,20,25].

CDW and electron doping

We use different electronic smearing parameters to simulate different temperatures. The obtained phonon dispersions are presented in Fig. 1d, e. At high temperatures, $NbSe_2$ and TaS_2 are stable with no negative frequency mode. While at low temperatures, there is a soft-mode band on ΓM, which is consistent with previous theoretical works[27–30]. This soft phonon mode is not caused by electron Fermi nesting. Instead, it is associated with EPC, and will lead to a CDW transition at low temperatures. To investigate electron doping effect, the electronic structures and phonon dispersions are computed for $NaNbX_2$ and 1H-MoX_2. The crystal structure of $NaNbSe_2$ is shown in the inset of Fig. 3b. It can be seen that Na atoms are intercalated between the layers. The 1e Wyckoff position in 1H-$NbSe_2$ corresponds to the 2c Wyckoff position in bulk $NaNbSe_2$. From its electronic structures and phonon dispersions in Fig. 3a, b, it shows that the empty-site EBR A_1'@2c is fully occupied and no negative phonon mode is found, suggesting a stable structure after Na intercalation. On the other hand, for Mo atoms substituting Nb atoms, the situation is similar: fully occupied empty-site EBR A_1'@1e leads to the absence of the negative phonon mode, as shown in Fig. 3c, d. The results in the electron-doped compounds reveal that the presence of soft phonon mode is related to the half filling of the empty-site EBR. The electron doping can stabilize the crystal structure and suppress CDW transition.

Superconductivity

To investigate the SC property, we calculated the electron-phonon couplings $\lambda_{\mathbf{q}\nu}$ with $\sigma = 0.02$ Ry, depicted by the magenta circles in Fig. 2c. It shows that the soft phonon mode near M point has the large $\lambda_{\mathbf{q}\nu}$. Further, the side and top views of the corresponding phonon vibration pattern at M point are plotted in Fig. 2d to analyze the EPC-favorable vibration mode. It shows that the soft phonon mode at M point is mainly from Nb atoms that only

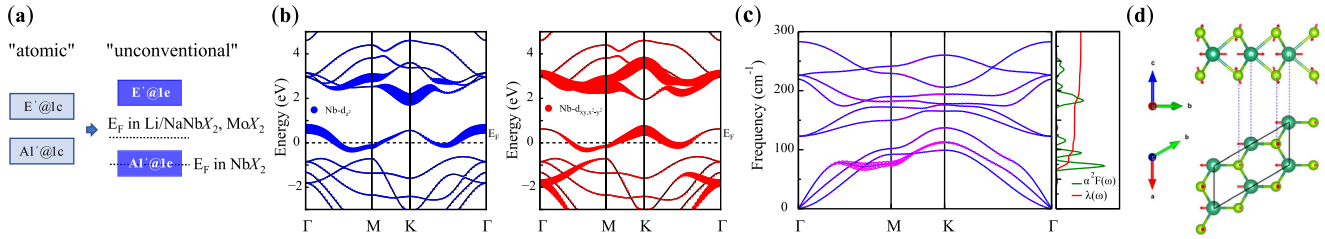

Fig. 2 The schematic of band hybridization, orbital-resolved band structures, and the phonon dispersions and vibration modes. a The schematic of the formation of the empty-site EBR A_1'@1*e* at E_F. It is formed by the hybridization of A_1'@1*c* (from Nb-d_{z^2}) and E'@1*c* (from Nb-d_{xy,x^2-y^2}) ABRs. **b** Orbital-resolved band structures in 1H-$NbSe_2$ with the corresponding Nb d_{z^2} and d_{xy,x^2-y^2} orbitals weights colored in blue and red, respectively. The size of the symbol represents the orbital weight. **c** The phonon spectrum of 1H-$NbSe_2$ with magenta circles representing EPC $\lambda_{\mathbf{q}\nu}$, and the Eliashberg spectral function $\alpha_2F(\omega)$, the frequency-dependent coupling $\lambda(\omega)$. **d** The phonon vibration mode of the lowest phonon band at *M* point.

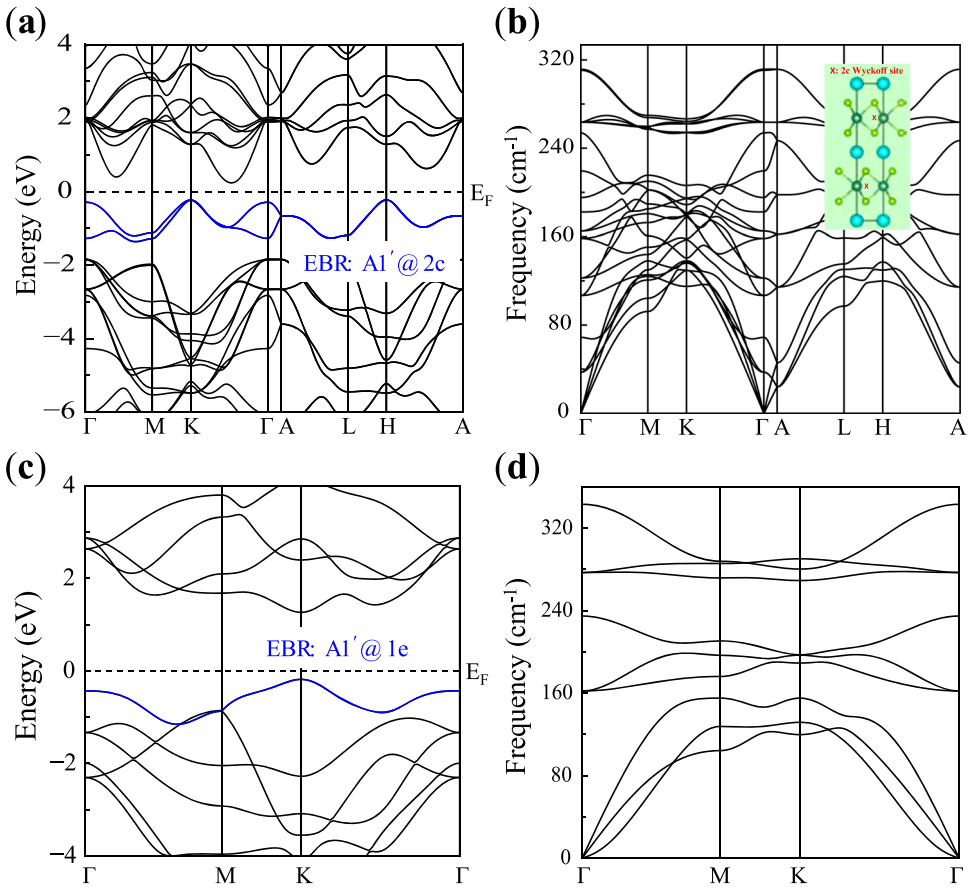

Fig. 3 Electronic structures and phonon dispersions after electron doping. Electronic structures and phonon dispersions of (**a**, **b**) bulk $NaNbSe_2$ and (**c**, **d**) 1H-$MoSe_2$. Inset in **b** presents the crystal structure of the bulk $NaNbSe_2$ with Na intercalation. The electron doping can stabilize the crystal structure.

vibrate in-plane. On the right of Fig. 2c, we calculated the Eliashberg spectral function $\alpha_2F(\omega)$ and the frequency-dependent coupling $\lambda(\omega)$. It can be seen that the contributions of

$$\lambda = \Sigma_{\mathbf{q}\nu}\lambda_{\mathbf{q}\nu} = 2\int_0^\infty d\omega \frac{\alpha^2F(\omega)}{\omega} \quad (2)$$

mainly come from the phonon modes near 70 cm^{-1}. Due to the existence of soft phonon modes near *M* point, the 1H-$NbSe_2$ hosts strong EPC ($\lambda > 1$)[31]. In the partially filling situation, the Fermi-level states are mainly centered at the empty site. On the other hand, this phonon mode strongly squeezes the empty site in Fig. 2d. The coincidence between phonon mode and the Fermi-level states gives rise to the strong EPC, eventually leading to the SC instability. Besides, the SC in $NbSe_2$ can be tuned through carrier doping and dimensionality, such as Li/Na/Cu intercalation or Mo/W substitution[32–34].

Prediction of superconductivity in TaNS monolayer and TaN_2 bulk

As the partial filling of the empty-site EBR can lead the strong EPC and SC. Following this way, we predicted the SC in unconventional metallic TaNS monolayer [the inset of Fig. 4a]. The electronic structure is shown Fig. 4a. There exists a half-filling empty-site EBR

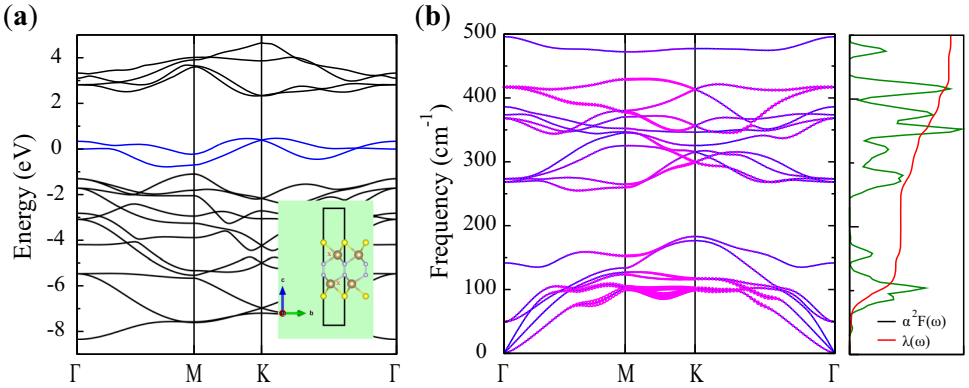

Fig. 4 Electronic structures, phonon dispersions, and electron-phonon couplings in TaNS monolayer. a Band structures of TaNS monolayer in SG 164. **b** Phonon spectrum, Eliashberg spectral functions $\alpha^2F(\omega)$, and the frequency-dependent coupling $\lambda(\omega)$. The electron-phonon couplings $\lambda_{\mathbf{q}\nu}$ are represented by magenta circles.

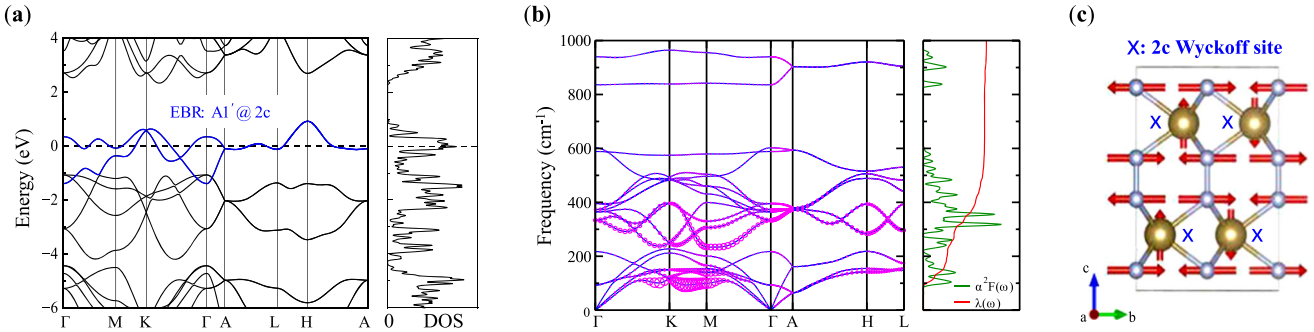

Fig. 5 Electronic structures, phonon dispersions, and electron-phonon couplings in bulk 2H-TaN_2. a Band structures and density of states of bulk 2H-TaN_2 in SG 194. The EBR of the low energy bands (in blue) is A_1'@2*c*, whose sites (indicated by "x" in **c**) are empty in crystals. **b** Phonon spectrum, Eliashberg spectral functions $\alpha^2F(\omega)$, and the frequency-dependent coupling $\lambda(\omega)$. The electron-phonon couplings $\lambda_{\mathbf{q}\nu}$ are represented by magenta circles. **c** The phonon vibration mode of lowest frequency at M.

at E_F, which is colored in blue. With the strong dimerization of N-N bonds, the band structure of TaNS shares a similar unconventional nature, with the electronic charge centers at empty sites (red crossings in the inset). The calculated phonon spectrum is shown in Fig. 4b. There are no imaginary frequencies in the phonon spectrum, indicating the stability of the structure. From the calculated electron-phonon couplings $\lambda_{\mathbf{q}\nu}$, Eliashberg spectral functions $\alpha_2F(\omega)$, and the frequency-dependent coupling $\lambda(\omega)$, it can be seen that the EPC constants λ are mainly contributed by the phonon modes near 100 cm^{-1}. The superconducting transition temperature (T_C) is estimated using Allen-Dynes modified McMillian equation[35,36],

$$T_C = \frac{\omega_{log}}{1.2k_B}\exp\left[\frac{-1.04(1+\lambda)}{\lambda(1-0.62\mu^*)-\mu^*}\right] \quad (3)$$

where k_B is the Boltzmann constant, μ^* is the effective screened Coulomb repulsion constant, typically ~ 0.1, λ is electron-phonon coupling constant, and ω_{log} is logarithmic average phonon frequency. With $\mu^* = 0.10$ and $\lambda = 0.72$, T_C of TaNS is estimated to be 10 K using Allen-Dynes modified McMillian equation.

Moreover, we predict another unconventional metal 2H-TaN_2 with superconductivity. Due to the dimerization of N-N bonds, they form the state of $(N_2)^{4-}$ in bulk TaN_2, resulting in the same situation of 2H-MX_2. The calculated electronic structure for bulk 2H-TaN_2 is presented in Fig. 5a. There exists a half-filling empty-site EBR, which is colored in blue. The computed phonon spectra indicated that 2H-TaN_2 is stable with $\sigma = 0.02$ Ry, as shown in Fig. 5b. 2H-TaN_2 was also proposed to be a metastable phase at high pressure using structure prediction method[37]. With $\mu^* = 0.10$ and $\lambda = 1.04$, T_C of bulk 2H-TaN_2 is estimated to be 26 K using Allen-Dynes modified McMillian equation, which is close to McMillan limit (~40 K). As the λ is compatible with conventional superconductors, the high ω_{log} is important in the final calculated T_C, which is mainly contributed from light mass N atoms. The phonon spectrum, and corresponding $\lambda_{\mathbf{q}\nu}$, $\alpha^2F(\omega)$, $\lambda(\omega)$ of 2H-TaN_2 are also shown in Fig. 5b. The contributions of $\lambda(\omega)$ mainly come from the phonon modes of $\omega < 400\ cm^{-1}$. Among these phonon modes, we find that the low frequency phonon modes (~100 cm^{-1}) along *K-M* high symmetry line show significant contribution to λ. The corresponding phonon vibration mode around *M* is shown in Fig. 5c. In this phonon mode, the Ta atoms vibrate along *z* direction, and the N atoms vibrate in *xy* plane, which has a higher amplitude than Ta atoms. It is noted that, the N atoms vibration modes along *z* direction have frequencies higher than 500 cm^{-1} because of strong N-N bonds. Thus, the in-plane vibration modes of N atoms couple with electride electron states around E_F, inducing high EPC constants.

Discussion

The unconventional metals with an empty-site EBR encompass intriguing correlated states due to the soft phonon mode and strong EPC. We find that 1H/2H-phase TMD MX_2 has a half-filled empty-site EBR at E_F. The strong EPC is associated with half filling of the empty-site A_1'@1*e* EBR near the Fermi level. The strong EPC may originate from the quantum geometric contributions of the unconventional electronic structure[38]; for example, the σ-bond band of MgB_2 belongs to the A_{1g}@3*f* EBR at empty sites with

partial filling. Our results indicate that the empty-site band in unconventional metals is crucial for electron-phonon coupling and superconductivity. Following this strategy, we predict unconventional metals TaNS monolayer and 2H-TaN_2 bulk with SC $T_C = 10$ K and 26 K respectively. It deserves further experimental focus and confirmation. In conclusion, our findings reveal that the partial filling of the empty-site EBR in unconventional metals can give rise to strong EPC, as the Fermi-level states and phonon modes coincide spatially. The unconventional metals provide an ideal platform to search for superconductors.

METHODS

Calculation method

We performed the first-principles calculations with QUANTUM ESPRESSO (QE) package[39] based on the density functional theory (DFT) with the projector-augmented wave (PAW) pseudopotentials[40,41]. The Perdew-Bruke-Ernzerhof (PBE) exchange-correlation functional of generalized gradient approximation was adopted. The dynamical matrices and electron-phonon coupling calculations were performed in the framework of density functional perturbation theory, as implemented in the QE package. The superconducting temperature was evaluated with Allen-Dynes modified McMillian equation using QE. The irreducible representations are computed by IR2PW[42].

DATA AVAILABILITY

All data are available from the corresponding author on reasonable requests.

CODE AVAILABILITY

All codes used for this work are open-source. The DFT calculations are based on QUANTUM ESPRESSO. IR2PW is available in https://github.com/zjwang11/IR2PW, which is used to compute the irreducible representation in QE. The POS2ABR is available at https://github.com/zjwang11/UnconvMat.

Received: 13 August 2023; Accepted: 14 January 2024;
Published online: 30 January 2024

REFERENCES

1. Qi, X. L. & Zhang, S.-C. The quantum spin Hall effect and topological insulators. *Phys. Today* **63**, 33 (2010).
2. Hasan, M. Z. & Kane, C. L. Colloquium: Topological insulators. *Rev. Mod. Phys.* **82**, 3045 (2010).
3. Bernevig, B. A., Hughes, T. L. & Zhang, S.-C. Quantum spin hall effect and topological phase transition in HgTe quantum wells. *Science* **314**, 1757 (2006).
4. Zhang, H. et al. Topological insulators in Bi_2Se_3, Bi_2Te_3 and Sb_2Te_3 with a single Dirac cone on the surface. *Nat. Phys.* **5**, 438 (2009).
5. Armitage, N. P., Mele, E. J. & Vishwanath, A. Weyl and Dirac semimetals in three-dimensional solids. *Rev. Mod. Phys.* **90**, 015001 (2018).
6. Wan, X., Turner, A. M., Vishwanath, A. & Savrasov, S. Y. Topological semimetal and Fermi-arc surface states in the electronic structure of pyrochlore iridates. *Phys. Rev. B* **83**, 205101 (2011).
7. Weng, H., Dai, X. & Fang, Z. Topological semimetals predicted from first-principles calculations. *J. Phys. Condens. Matter.* **28**, 303001 (2016).
8. Wang, Z., Weng, H., Wu, Q., Dai, X. & Fang, Z. Three-dimensional Dirac semimetal and quantum transport in Cd_3As_2. *Phys. Rev. B* **88**, 125427 (2013).
9. Wang, Z. et al. Time-reversal-breaking Weyl fermions in magnetic heusler alloys. *Phys. Rev. Lett.* **117**, 236401 (2016).
10. Nie, S. et al. Topological phases in the $TaSe_3$ compound. *Phys. Rev. B* **98**, 125143 (2018).
11. Kumar, N. et al. Signatures of sixfold degenerate exotic fermions in a superconducting metal $PdSb_2$. *Adv. Mater.* **32**, 1906046 (2020).
12. Qian, Y. et al. Topological electronic states in HfRuP family superconductors. *npj Comput. Mater.* **5**, 121 (2019).
13. Gao, J. et al. Unconventional materials: the mismatch between electronic charge centers and atomic positions. *Sci. Bull.* **67**, 598 (2022).
14. Nie, S. et al. Application of topological quantum chemistry in electrides. *Phys. Rev. B* **103**, 205133 (2021).
15. Xu, Y. et al. Three-dimensional real space invariants, obstructed atomic insulators and a new principle for active catalytic sites. Preprint at https://arxiv.org/abs/2111.02433 (2021a).
16. Bradlyn, B. et al. Topological quantum chemistry. *Nature* **547**, 298 (2017).
17. Po, H. C., Watanabe, H. & Vishwanath, A. Fragile topology and Wannier obstructions. *Phys. Rev. Lett.* **121**, 126402 (2018).
18. Song, Z.-D., Elcoro, L. & Bernevig, B. A. Twisted bulk-boundary correspondence of fragile topology. *Science* **367**, 794 (2020).
19. Xu, Y, et al. Filling-enforced obstructed atomic insulators. Preprint at https://arxiv.org/abs/2106.10276 (2021b).
20. Li, G. et al. Obstructed surface states as the descriptor for predicting catalytic active sites in inorganic crystalline materials. *Adv. Mater.* **34**, 2201328 (2022).
21. Gao, J. et al. Electronic structures and topological properties in nickelates $Ln_{n+1}Ni_nO_{2n+2}$. *Natl. Sci. Rev.* **8**, nwaa218 (2020).
22. Wu, H. et al. The field-free Josephson diode in a van der Waals heterostructure. *Nature* **604**, 653 (2022).
23. Castro Neto, A. H. Charge density wave, superconductivity, and anomalous metallic behavior in 2D transition metal dichalcogenides. *Phys. Rev. Lett.* **86**, 4382 (2001).
24. Suderow, H., Tissen, V. G., Brison, J. P., Martínez, J. L. & Vieira, S. Pressure induced effects on the Fermi surface of superconducting 2H − $NbSe_2$. *Phys. Rev. Lett.* **95**, 117006 (2005).
25. Zhang, R., Sheng H., Deng J., Yang Z., & Wang, Z. Unconventional phonon spectra and obstructed edge phonon modes. Preprint at https://arxiv.org/abs/2305.09453 (2023).
26. Yadav K., Lamba M., Singh M., Kumar A., & Patnaik, S. Conventional type-II superconductivity in 2H-TaSeS. Preprint at https://arxiv.org/abs/2308.05377 (2023).
27. Weber, F. et al. Extended phonon collapse and the origin of the charge-density wave in 2H-$NbSe_2$. *Phys. Rev. Lett.* **107**, 107403 (2011).
28. Calandra, M., Mazin, I. I. & Mauri, F. Effect of dimensionality on the charge-density wave in few-layer 2H-$NbSe_2$. *Phys. Rev. B* **80**, 241108 (2009).
29. Lian, C.-S. et al. Intrinsic and doping-enhanced superconductivity in monolayer 1H-TaS_2 : Critical role of charge ordering and spin-orbit coupling. *Phys. Rev. B* **105**, L180505 (2022).
30. Bianco, R., Errea, I., Monacelli, L., Calandra, M. & Mauri, F. Quantum enhancement of charge density wave in NbS_2 in the two-dimensional limit. *Nano Lett.* **19**, 3098 (2019).
31. Jiang, C., Beneduce, E., Baggioli, M., Setty, C. & Zaccone, A. Possible enhancement of the superconducting T_c due to sharp Kohn-like soft phonon anomalies. *J. Phys. Condens. Matter.* **35**, 164003 (2023).
32. Li, L. et al. Superconductivity of Ni-doping 2H-TaS_2. *Phys. C* **470**, 313 (2010).
33. Liu H., Huangfu S., Lin H., Zhang X., & Schilling, A. Superconductivity in hydrated $Li_x(H_2O)_yTaS_2$. Preprint at https://arxiv.org/abs/2202.07725 (2022).
34. Zhang, H. et al. Tailored Ising superconductivity in intercalated bulk $NbSe_2$. *Nat. Phys.* **18**, 1425 (2022).
35. McMillan, W. L. Transition temperature of strong-coupled superconductors. *Phys. Rev.* **167**, 331 (1968).
36. Allen, P. B. & Dynes, R. C. Transition temperature of strong-coupled superconductors reanalyzed. *Phys. Rev. B* **12**, 905 (1975).
37. Xing, W., Wei, Z., Yu, R. & Meng, F. Prediction of stable high-pressure structures of tantalum nitride TaN_2. *J. Mater. Sci. Technol.* **35**, 2297 (2019).
38. Yu, J. et al. Nontrivial quantum geometry and the strength of electron-phonon coupling. Preprint at https://arxiv.org/abs/2305.02340 (2023).
39. Giannozzi, P. et al. QUANTUM ESPRESSO: a modular and open-source software project for quantum simulations of materials. *J. Phys. Condens. Matter.* **21**, 395502 (2009).
40. Blöchl, P. E. Projector augmented-wave method. *Phys. Rev. B* **50**, 17953 (1994).
41. Kresse, G. & Joubert, D. From ultrasoft pseudopotentials to the projector augmented-wave method. *Phys. Rev. B* **59**, 1758 (1999).
42. Zhang, R. et al. Large shift current, π Zak phase, and the unconventional nature of Se and Te. *Phys. Rev. Res.* **5**, 023142 (2023).

ACKNOWLEDGEMENTS

This work was supported by the National Key R&D Program of China (Grants No. 2023YFA1607401, No. 2022YFA1403800), the National Natural Science Foundation of China (Grants No. 11974395, No. 12188101), the Strategic Priority Research Program of Chinese Academy of Sciences (Grant No. XDB33000000), and the Center for Materials Genome.

AUTHOR CONTRIBUTIONS

Z.W. proposed and supervised the project. Z.Y., H.S., R.Z. and Z.G. conducted the theoretical calculations. All authors contributed to analyzing the results and writing the manuscript.

COMPETING INTERESTS

The authors declare no competing interests.

ADDITIONAL INFORMATION

Correspondence and requests for materials should be addressed to Zhijun Wang.

Reprints and permission information is available at http://www.nature.com/reprints

Publisher's note Springer Nature remains neutral with regard to jurisdictional claims in published maps and institutional affiliations.